Materials Today Communications 38 (2024) 107858

Contents lists available at ScienceDirect

Materials Today Communications

journal homepage: www.elsevier.com/locate/mtcomm

Antimicrobial efficacy of solar disinfection in cellulose fiber supported photoactive materials

Daniel Langerreiter [a], Katariina Solin [b], Mireia Jordà-Redondo [c], Roger Bresolí-Obach [c], Lukas Fliri [a], Santi Nonell [c,*], Mauri A. Kostiainen [a,*], Eduardo Anaya-Plaza [a,*]

[a] Department of Bioproducts and Biosystems, Aalto University, Kemistintie 1, 02150 Espoo, Finland
[b] Bioinspired Materials, VTT Technical Research Centre of Finland Ltd., FI-02044 Espoo, Finland
[c] Institut Químic de Sarrià Universitat Ramon Llull, Via Augusta 390, 08017 Barcelona, Spain

ARTICLE INFO

Keywords:
Cellulose nanofibers
Photodynamic inactivation
Toluidine blue
Singlet oxygen
Solar disinfection

ABSTRACT

According to the World Health Organization, antimicrobial resistance is one of the emerging threats to global health. Therefore, the development of new strategies to mitigate resistant bacterial strains is highly desirable. Photodynamic inactivation is a promising approach owing to its effectiveness against a broad range of microorganisms irrespective of their antibiotic resistance profile and its multitarget mechanism that hamper the appearance of acquired resistance. In this work, a self-sterilizing and potentially biodegradable material is developed, providing a green alternative for single-use packaging in the medical, food, and cosmetic industry. We demonstrate two synthetic approaches based on covalent linkage of toluidine blue to tempo-oxidized carbon nanofibers, as well as the supramolecular immobilization based on electrostatic self-assembly. The former shows high activity, reaching inactivation rates of 8 Log_{10} CFU for *S. aureus* and *E. coli* after 15 min under 250 $W{\cdot}m^{-2}$ artificial sun irradiation. This simple and facile approach will enable the preparation of composite photoantimicrobial films that are light activated, providing clean and microbiologically safe surfaces, even in challenging situations, such as natural disasters or conflicts, or remote locations with of none or limited access to other forms of energy supply.

1. Introduction

Antibiotic resistance is an emerging threat that needs to be tackled urgently. According to the World Health Organization (WHO), it is a pressing menace to global development, health and food safety. An increasing number of multi-resistant microorganisms (MROs) such as the methicillin-resistant *Staphylococcus aureus* or *Escherichia coli* bacteria, or the *Candida* yeasts, have been detected,[1] with an acute impact in e.g. healthcare units, hospitals or elderly care homes, where an MRO infection can be lethal. Therefore, the development of new antimicrobial approaches is urgently required. Among the recently-developed antimicrobial strategies, photodynamic inactivation (PDI) shows a high potential due to its broad-spectrum efficiency, ubiquitous activation path via visible light, susceptibility towards antibiotic-resistant strains, and low potential for developing resistance derived from its multi-target mechanism of action.[2] As the sun is the main source of natural light, PDI is a valuable option in critical situations such as natural disasters, or in remote locations where no additional power supply is available.[3–8] PDI has been reported as an effective method to inactivate a broad spectrum of pathogens, including MROs, both in planktonic and biofilm stages. It relies on the photoactivation of a dye, referred to as photosensitizer (PS) to generate long-lived triplet excited states, which subsequently transfers the acquired photon energy to suitable substrates such as molecular oxygen present in the media. This photochemical process often generates reactive oxygen species (ROS) such as singlet oxygen ($^1O_2$) that are capable of oxidizing different biomolecules, rendering a broad-spectrum irreparable damage that hampers the appearance of photo-resistant strains.[9–11]

Toluidine blue (TB), also known as basic blue 17, is a thiazine metachromatic dye widely used in histology as a stain, particularly of polysaccharides present in plant cells, as well as in clinical practice to image premalignant lesions.[12–14] TB is also a cationic photosensitizer with strong absorption in the red area of visible light and high capacity to produce $^1O_2$, therefore it has attracted interest of the photodynamic inactivation community.[15–18] Additionally, TB is commercially available and can be used without any additional structural

* Corresponding authors.
E-mail addresses: santi.nonell@iqs.url.edu (S. Nonell), mauri.kostiainen@aalto.fi (M.A. Kostiainen), eduardo.anaya@aalto.fi (E. Anaya-Plaza).

https://doi.org/10.1016/j.mtcomm.2023.107858
Received 16 October 2023; Received in revised form 30 November 2023; Accepted 11 December 2023
Available online 19 December 2023

modification, rendering a prime PS.[19]

However, even if PDI is gaining momentum and attracting the efforts of the scientific and medical communities, there is a need for the development of single-use packaging bearing MRO-free surfaces, while maintaining a sustainable and environmentally benign approach. In this respect, tempo-oxidized cellulose nanofibers (TOCNF)[20–22] can be used as an environmentally friendly matrix material for attaching TB. Due to the numerous inherent qualities of cellulosic nanomaterials, such as availability, potential biodegradability, and biocompatibility, they exhibit broad potential for developing advanced functional materials from sustainable and renewable resources.[23–25] Consequently, nanocelluloses have been demonstrated to improve functionality in various applications ranging from active thin-films[26,27] to active composites [28–30] and multi-layered structures.[31–33] In particular, cellulosic materials have shown great potential as scaffolds for photodynamic inactivation, due to the previously mentioned properties. The synthesis of such hybrid materials can be divided in two different strategies: covalent and supramolecular immobilization. The former yields stable derivatives with neglectable migration of the PS to the substrate, while the latter is more synthetically accessible. On the one hand, the covalent modifications, which can be done via different synthesis pathways like EDC-NHS chemistry[34], esterification[35], Cu (I)-catalyzed Huisgen-Melal-Sharpless 1,3-dipolar cycloaddition[36,37], conjugation through 2,4,6-trichloro-1,3,5-triazin typical of the dye industry [37–40], biosynthesis[41] or conjugation through DMT activation.[42] On the other hand, the supramolecular approach is used as well due to the electrostatic interaction of the cationic photosensitizers and the anionic cellulosic material.[43–46].

Here, we report two strategies to load TOCNFs with TB. Primarily, covalent binding via EDC/NHS coupling is investigated. In addition, a supramolecular approach based on electrostatic interactions of the positively-charged TB and the negatively charged TOCNF is explored as well.[45] The benefits and downsides of both approaches are investigated and compared. It was found that the covalent approach yields more reliable photoinactivation performance, rendering a more suitable candidate for applications in packaging or coatings.

2. Results and discussion

2.1. Preparation and characterization of TB-doped nanocellulose materials

We investigated two methods for incorporating TB into TOCNF. TB was either covalently conjugated to TOCNF (**1**) via EDC/NHS chemistry (Fig. 1a), or physically adsorbed onto the TOCNF fiber network (**2**; Fig. 1b). Our primary focus was on the covalently bound sample, which prevents the photosensitizer from leaching out of the material and therefore makes it safer for usage. After purification, which consisted of different washing steps described in the SI and dialysis, the resulting samples were kept in solution to avoid aggregation upon drying-redispersion cycles. We characterized both samples using surface plasmon resonance (SPR), attenuated total reflectance infrared spectroscopy (ATR-IR), and UV-Vis spectroscopy. Both conjugates **1** and **2** exhibited a blue/purple color, as observed by the naked eye, as consequence of the successful immobilization of TB (Fig. 1, bottom).

The FTIR spectra of covalently linked TB-TOCNF (**1**), physically adsorbed TB-TOCNF (**2**), together with TB and TOCNF as controls are shown in Fig. 2a. The characteristic Gaussian shaped peak at 1602 cm^{-1} can be assigned to the C═O stretching vibration of the carboxylic acids from the TOCNF. The additional peaks of **1** at 1650 and, particularly 1693 cm^{-1} evolving underneath the curve of the C═O stretching vibration band of TOCNF, are assigned to an amide bond (amide I) C═O stretch, well in line with the successful amidation of TOCNF. Note that the peak at *c.a.* 1602 cm^{-1} that remains in spectra is assigned to unreacted carboxylates for **1** and **2** (Fig. 2a, blue and green respectively), and the NH bending of the primary aromatic amine for **TB** (Fig. 2a, red).

First, fundamental confirmation of the mechanism of binding was obtained by conjugation of TB on TOCNF thin films in-situ by SPR (Fig. 2b). The adsorption curves of TB on pristine TOCNF (as reaction pathway for **2**) and coupling to EDC/s-NHS activated surfaces (as reaction pathway for **1**) can be seen in Fig. 2b. First, the TOCNF film is reacted with EDC/s-NHS (see Supporting Information for detailed experimental details), observing a *c.a.* 0.4° after washing, following a typical curve for the activation of nanocellulose.[47,48] This increase is caused by two factors: the EDC grafting after EDC/s-NHS coupling as well as thin film swelling, with the consequent enhanced water

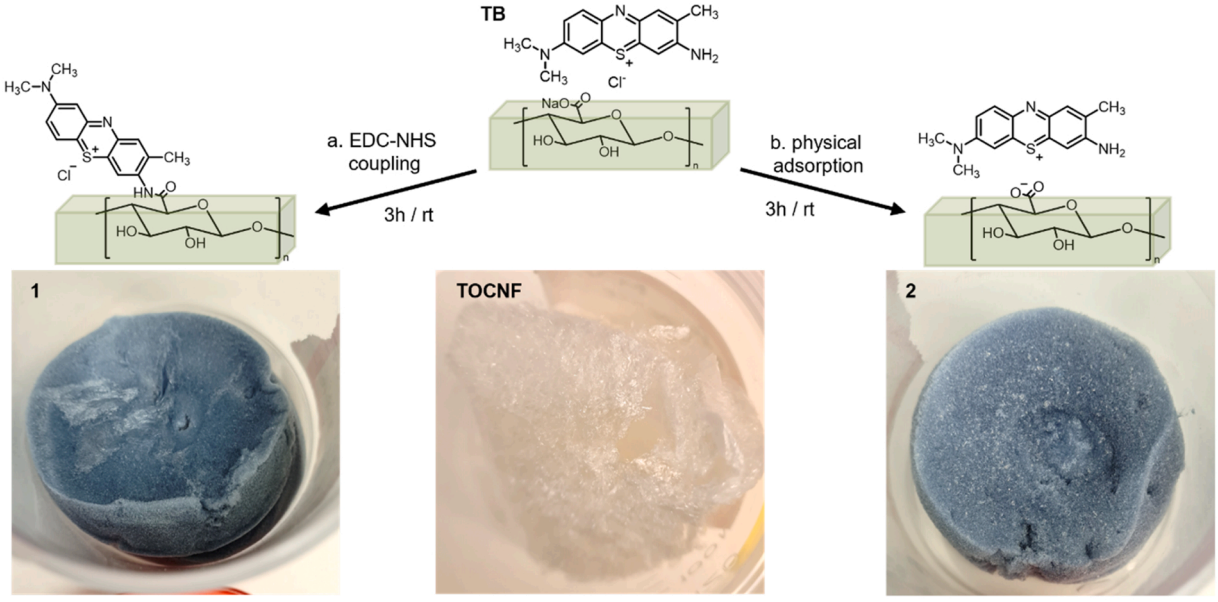

Fig. 1. Synthesis (top) of the antibacterial cellulosic hybrid material by a) covalent modification of tempo-oxidized cellulose nanofibers (TOCNF) with toluidine blue (TB) via EDC NHS coupling (**1**) and b) physical adsorption (**2**) through mixing. Photographs (bottom) of the freeze-dried material.

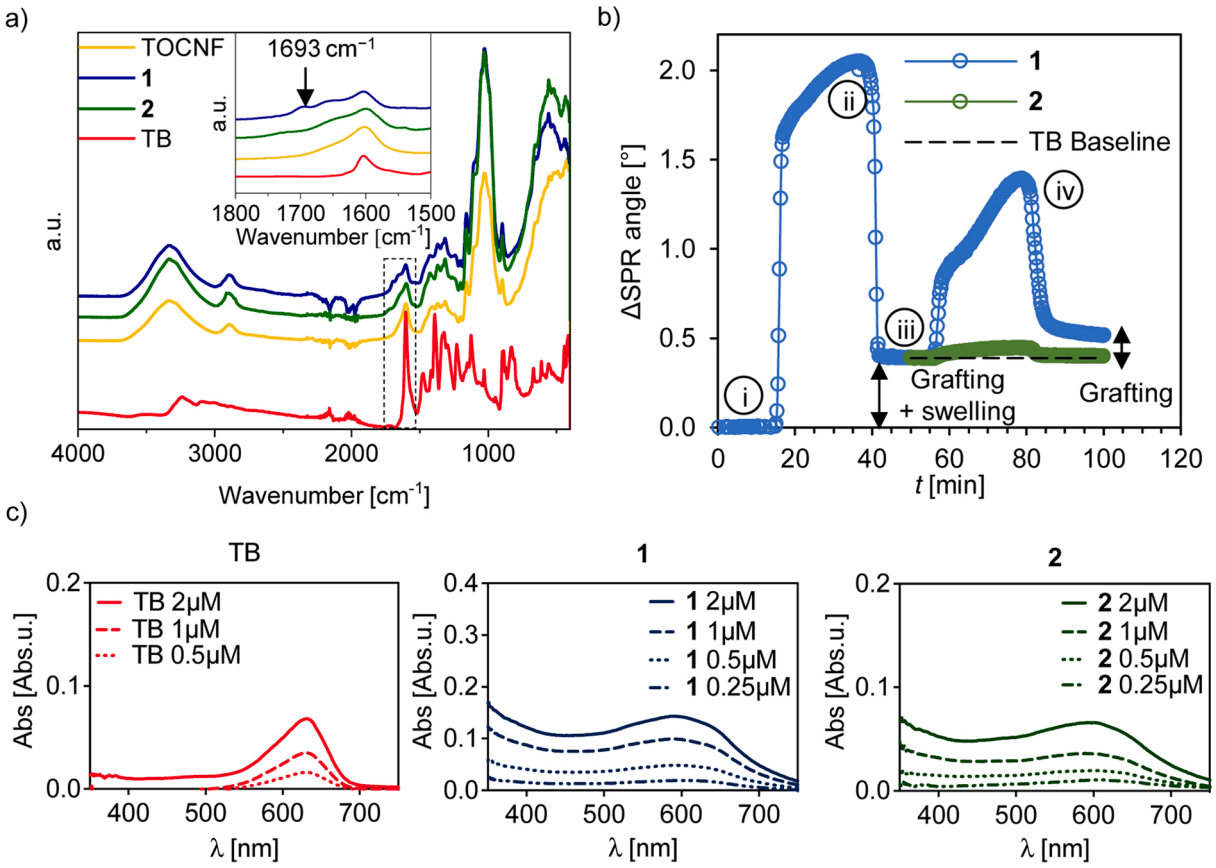

Fig. 2. Samples characterization. a) Stacked FTIR spectra with TOCNF (yellow) **1** (blue) and **2** (green) and TB (red). b) SPR sensogram shows i) EDC grafting for **1** (blue), ii) washing of unbound material, iii) grafting of TB for **1** and **2** (blue and green), and iv) washing of unbound material. TB adsorbs weakly onto pristine TOCNF surface while significant coupling was obtained via covalent conjugation. c) UV-Vis of TB, **1**, **2** at different concentrations show the different absorption maxima and peak width depending on the aggregation of the material.

absorption. After EDC/s-NHS activation (Fig. 2b), significant adsorption of TB was observed indicating immobilization of the dye through chemical bond to the activated nanocellulose surface. Interestingly, the washing process eliminates loosely adsorbed material, and indicates a low reaction yield resulting from either low reactivity or low accessibility to the surface. Nevertheless, **1** shows 11.0 mg m^{-2} of bound TB after washing, around one order of magnitude higher retention when compared to **2** (0.7 mg m^{-2}). However, the apparent higher payload for **1** compared to **2** is likely due to the swelling observed in the EDC/s-NHS activation step, greatly increasing the surface available for reaction, as opposed to the tightly packed film for **2**. Therefore, in order to characterize the TB payload on the cellulosic material, UV-Vis absorption measurements were performed, using TB at different concentrations as calibration curve (Fig. S1). The UV-Vis absorption spectra presented in Fig. 1c, show the typical absorption peak of TB at 635 nm. Both cellulosic samples show broader peaks, which imply TB interaction with the TOCNF network. This limits the accurate determination of the payload, although allows estimations and, more importantly, serves to compare payload between the two synthetic approaches. TB payload for **1** and **2** was estimated to be 2.3 and 5.6 mg per g of TOCNF, which correspond to an 8.2% and 20.2% coverage of the carboxylate reaction sites, respectively (either covalently or charge-neutralized). The ζ-potential is well aligned with these measurements: the unmodified TOCNF showed the highest negative charge with − 49.7 ± 8.9 mV. The covalently linked sample **1** with a value of − 43.7 ± 1.2 mV shows less negative surface charge, which indicates a partial, yet minor neutralization of carboxylates. The physically adsorbed sample **2** shows even less negative surface charge with − 39.0 ± 1.5 mV, as expected from the higher payload observed. In general lines, the changes observed are small, which indicates a low payload, in good agreement with previous characterization techniques. This, however, is beneficial for our approach, since the maintained high charge density renders colloidal stability of the fibers, therefore ensuring their processability.

Further insight into the film formation was achieved by microscopy. Fig. 3 shows AFM and SEM images of the spin-coated thin films and self-standing films of the prepared samples, respectively. The spin-coated TOCNF film (Fig. 3a) was uniform and very smooth (Rq roughness 0.83 nm) consisting of a loose distribution of nanofibrils. The conjugates **1** and **2** in turn formed much rougher films with visible aggregates. The highest roughness (Rq roughness 3.81 nm) and the biggest aggregates were observed with the **2** film. The conjugated film, **1**, was slightly smoother than the physical conjugate (Rq roughness 3.01 nm). Notably, since imaging was done in dry conditions, water removal most likely affected the formation of aggregations. The SEM images of self-standing films (Fig. 3d-f) show the topographical differences between pristine TOCNF and the conjugates on a larger scale. Similarly, as observed in AFM with the thin films, the thicker, self-standing TOCNF films were smooth, while larger fibril and particle aggregations could be observed in the TB modified films. Most likely, the addition of TB disrupts the electrostatic repulsion between cellulose nanofibrils contributing to the formation of homogeneous and stable nanocellulose suspensions. Therefore, the modified cellulosic materials show aggregation in the nanoscale that results in rougher film structures.

2.2. Photophysics of TB-doped nanocellulose materials

After physico-chemical characterization of the TB-doped nanocellulose materials, their photophysical properties were studied in detail

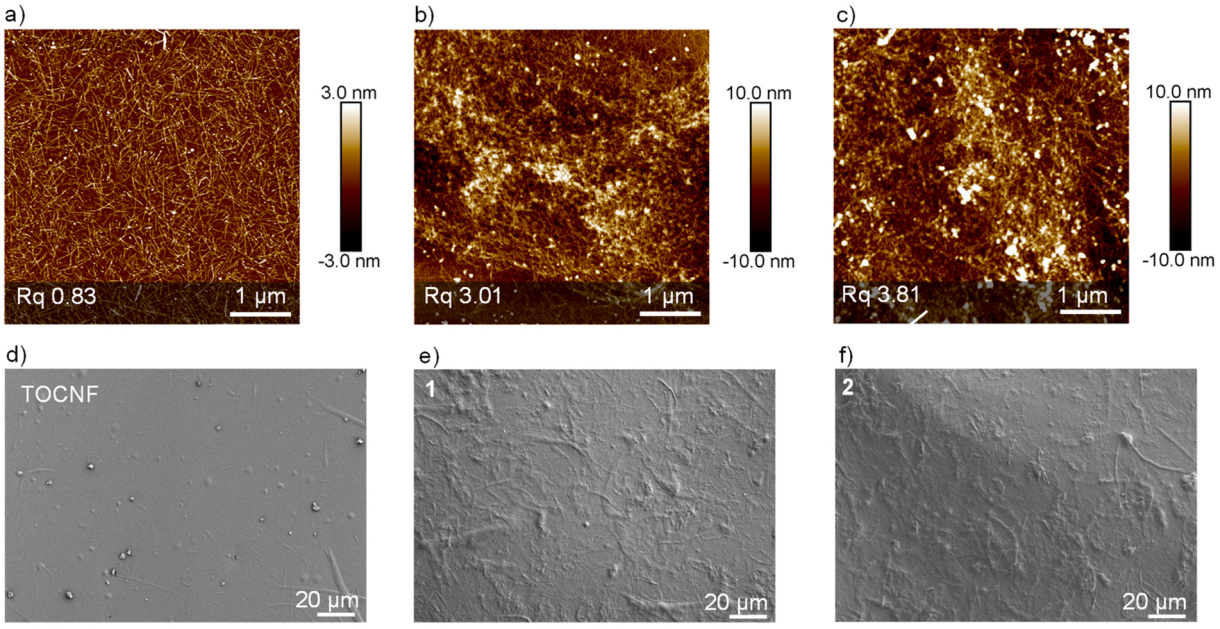

Fig. 3. Microscopy imaging of thin films. AFM height images with indicated roughness (Rq) of a) TOCNF, b) **1** and c) **2** thin films. SEM micrographs of d) TOCNF, e) **2**, and f) **1** self-standing films.

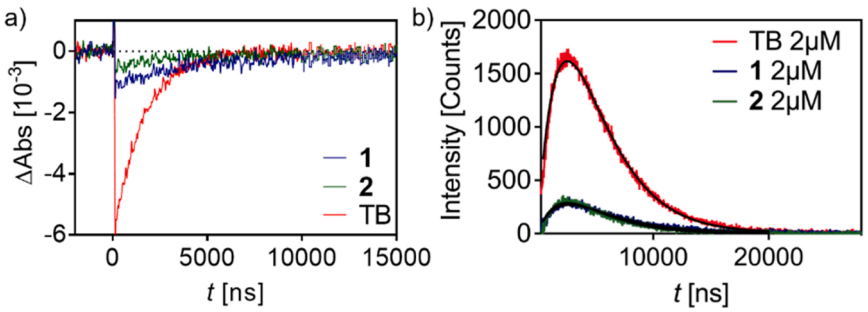

Fig. 4. Photophysical characterization of TB (red line), **1** (blue line) and **2** (green line) aerated 2 mM aqueous solution/suspension. a) Transient ground-state bleaching absorption traces. $\lambda_{Exc} = 355$ nm; $\lambda_{Obs} = 620$ nm. b) Singlet oxygen phosphorescence kinetic traces obtained by subtraction of the 1275 nm phosphorescence signal in absence and presence of 25 mM NaN_3. The raw phosphorescence signals are shown in Fig. S2. The black lines are the fit of equation S3 to the data $\lambda_{Exc} = 355$ nm.

(Fig. 4). On one hand, transient absorption experiments were performed to determine the lifetime of TB triplet excited state (τ_T) alone or loaded with TOCNF (Fig. 4a and Table 1). Since the TB triplet state is the precursor for $^1O_2$ generation, τ_T provides information about the O_2 accessibility to TB in the nanomaterial. Free TB shows a τ_T of 1.6 µs in aerated water, which is similar to the typical values of phenothiazinium photosensitizers dissolved in neat water.[49,50] Instead, **1** and **2** have longer τ_T, 3.4 and 2.8 µs, respectively, indicating that the TOCNF scaffold shields TB and hampers its interaction with O_2, specially for the covalently-attached material **1**. The intensity of the transient absorption difference signals (ΔAbs) is proportional to the quantum yield of triplet-state formation (Φ_T). For solutions containing equal concentrations of TB, ΔAbs is approximately 6-fold smaller when TB is attached to the TOCNF scaffold than in solution TB. Hence, the TB aggregation onto the TOCNF surface reduces its ability to generate the triplet state.

Using time-resolved near-infrared spectroscopy we observed that pulsed-laser irradiation at 532-nm of TB, **1** and **2** suspensions in water produced clear $^1O_2$ phosphorescence signals at 1275 nm (Fig. 4b).[51,52] Although all the three kinetic traces had the expected rise and decay shape of $^1O_2$ signals, the signals of samples **1** and **2** had an additional short-lived component due to the excitation light scattering by the TOCNF. Indeed, this scattering contribution hampers the fitting of the standard $^1O_2$ phosphorescence rise and decay kinetics described by Eq. (1), where τ_T and τ_Δ are the lifetimes of the photosensitizer triplet state and of $^1O_2$, respectively, and $S(0)$ is a quantity proportional to the $^1O_2$ production quantum yield (Φ_Δ).

$$S(t) = S(0) \quad x \quad \left(\frac{\tau_\Delta}{\tau_\Delta - \tau_T}\right) \quad x(e^{-t/\tau_\Delta} - e^{-t/\tau_T}) \tag{1}$$

Table 1
Lifetime and relative quantum yields of formation for TB triplet state (Φ_T), and $^1O_2$ (Φ_Δ) in aerated aqueous solutions/suspensions of free TB, **1** and **2**. The concentration of TB was 2 mM in all the experiments. Samples were excited at 532 nm, the triplet-triplet transient absorption was observed at 620 nm and $^1O_2$ phosphorescence at 1275 nm.

	Triplet TB			Singlet oxygen	
	τ_T / µs[a]	τ_T / µs[b]	Φ_T[a]	τ_Δ / µs[b]	Φ_Δ[b]
Free TB	1.6 ± 0.2	1.9 ± 0.2	1.0	3.2 ± 0.2	1.0
1	3.4 ± 0.2	3.6 ± 0.2	0.16 ± 0.02	2.2 ± 0.2	0.16 ± 0.02
2	2.8 ± 0.2	2.8 ± 0.2	0.17 ± 0.02	2.1 ± 0.2	0.20 ± 0.02

[a] From transient absorption spectroscopy.
[b] From time-resolved near-infrared phosphorescence spectroscopy.

Recording the signal in the presence of 20 mM NaN_3 (a well-known $^1O_2$ quencher[53]) allowed to isolate the contribution of scattering (Fig. S2). The actual contribution of $^1O_2$ to the 1275 nm signals was then obtained by subtracting the signals recorded in the absence and in the presence of azide (Fig. 4a and Table 1). By comparing the $S(0)$ values for the three samples, it was observed that the quantum yield of $^1O_2$ production by **1** and **2** is approximately 6-fold smaller than for free TB, consistent with the observed decrement in the triplet quantum yields. The τ_T obtained by TRNIR are in excellent agreement with those obtained by transient absorption. Regarding $^1O_2$, free TB has a τ_Δ of 3.2 μs, which is in agreement with the reported lifetime of $^1O_2$ in neat water. [54] Instead, **1** and **2** show smaller τ_Δ values 2.2 and 2.1 μs, respectively, which indicates that $^1O_2$ is partially quenched by the TOCNF host material.

2.3. Photobactericidal activity of TB-doped nanocellulose materials

Although the attachment of TB onto TOCNF reduces the photosensitizing properties of TB, these TB-cellulosic materials clearly retain potential for PDI purposes. The photoinactivation studies were performed on *Staphylococcus aureus* and *Escherichia coli* as a representative model of Gram-positive and Gram-negative bacteria, respectively (Fig. 5a). All studies were carried out in the dark and under light irradiation (630 nm red LED lamp and 300–800 nm solar simulator; Fig. 5). Each sample was measured at several TB concentrations up to 2 μM.

In a first series of experiments, the photoantimicrobial tests were performed under red light irradiation using **1** (blue), **2** (green) and the controls TB (red) and TOCNF (orange) delivering a light fluence of 20 J cm^{-2} (Fig. 5a). Since none of the materials showed dark toxicity on bacteria, only the dark control of TB is shown in Fig. 5 for clarity purposes. The others are presented in the supporting information (Fig. S3). We selected mild photodynamic therapy conditions, including short incubation times and low concentrations, to effectively kill typical microbes. These conditions aim to minimize unnecessary damage to the surrounding host tissue as PDT treatments on mammalian cells typically require stronger conditions, thereby reducing the potential side effects of PDT treatment.[55].

First, is worth noticing that TOCNF shows no phototoxicity, as expected given absence of photosensitizer. In *S. aureus*, both free TB and **1** show a similar photoinactivation activity, achieving a reduction of 5–6 $\log_{10}$ in colony-forming units (CFU mL^{-1}) at 2 μM TB. Instead, the **2** achieves a more modest photoinactivation outcome (only 2 $\log_{10}$ CFU mL^{-1} at 2 μM). *E. coli* was less susceptible than *S. aureus* to the photodynamic treatments due to both the more complex cellular wall and the electrostatic barrier posed by the negative charges of the TOCNF and the bacterial surfaces. **1** was clearly more efficient than free TB at low concentrations, although both agents achieved a reduction of almost 5 $\log_{10}$ CFU mL^{-1} at 2 μM. Interestingly, **2** was more active against *E. coli* than *S. aureus*. These results highlight the potential of the TOCNF scaffold for photoantimicrobial purposes, particularly for **1**, which shows similar (or even a slightly better) photodynamic activity than free TB despite its negative ζ-potential and lower capacity to generate $^1O_2$. Inspired by these positive results, we also tried to photoinactivate the opportunistic pathogenic yeast *Candida albicans*, however with negative results in all cases (Fig. S4). Note that despite *C. albicans* is a eukaryotic cell, we did not modify the incubation time of TB. This decision is based on reports indicating that the uptake of TB by *C. albicans* typically occurs within 10–15 min. [56–60]. Moreover, our materials are specifically engineered for surface applications, aimed at eliciting a photoantimicrobial response without photosensitiser internalisation.

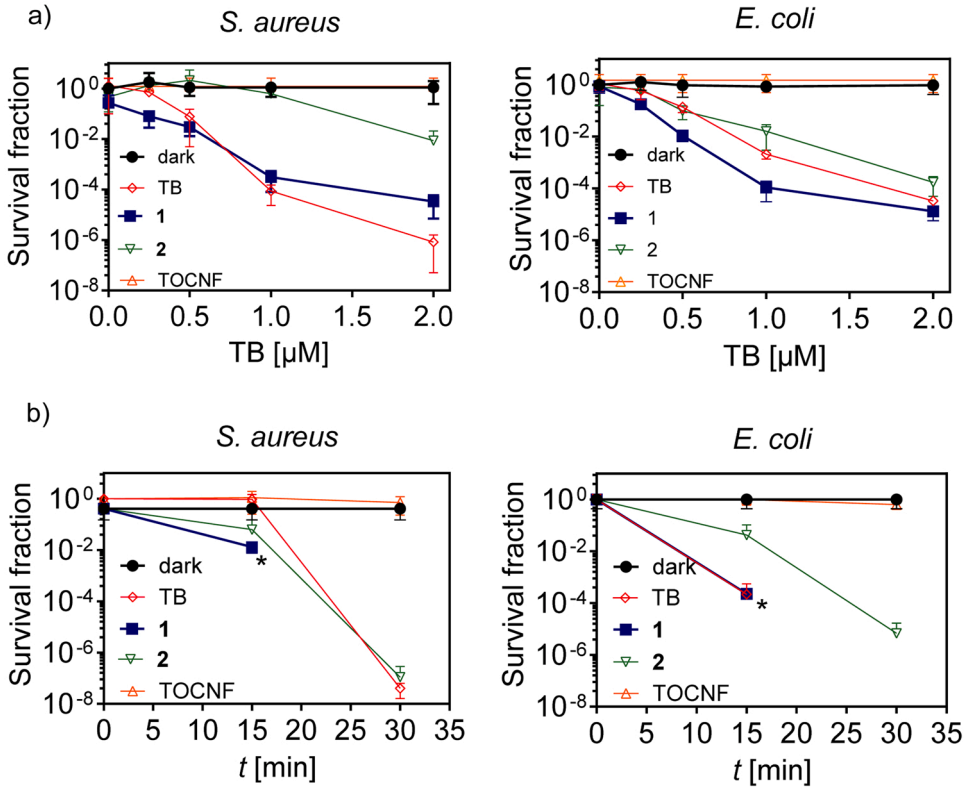

Fig. 5. Survival curves of Staphylococcus aureus (left), and Escherichia coli (right). a) Samples incubated with different concentrations of **TB** (red circles), **1** (blue square), **2** (green down triangle) and TOCNF (orange up triangle) irradiated with red light (λ = 635 ± 10 nm; 20 J·cm^{-2}). b) Samples incubated at 2 μM TB and receiving increasing solar light irradiation time (SuntestXLS+; λ = 300–800 nm; 250 W·m^{-2}). For clarity, a single non-irradiated (dark) control (TB) is shown for each assay, the others non-irradiated (dark) controls are shown in Fig. S3. Data are shown as mean ± SD of n = 18 replicates. *After 15 min 8 $\log_{10}$ CFU mL^{-1} were killed, and no bacteria left to measure. Data is shown as the ratio between the counted cells and the maximum attainable cell count under dark conditions (dark control), reflecting the relative survival rate in dimensionless units.

To achieve a figure of merit for photoantimicrobial TOCNF, these materials were also tested using a solar simulator configured for outdoor daylight. We set an irradiance of 250 W/m^2 in the 300–800 nm range, which is roughly 50% of the standard global solar irradiance at sea level. [61] Under this polychromatic irradiation, **1** was able to photoinactivate almost 2 $\log_{10}$ of *S. aureus* within only 15 min of irradiation, while **2** and free TB showed negligible phototoxicity. More striking are the results after 30 min of simulated solar irradiation, where **1** reduced the *S. aureus* bacterial count by more than 8 $\log_{10}$ CFU mL^{-1}, while **2** and free TB alone could achieve 7 $\log_{10}$ CFU mL^{-1} reduction. Strikingly, the assay on *E. coli* revealed an even higher bactericidal efficiency of TB and **1** under sunlight exposure relative to *S. aureus*, namely 3 $\log_{10}$ CFU mL^{-1} reduction (>99.9%) after only 15 min of simulated solar irradiation. The higher bacterial effects of 1 on *E. coli* arise out of its nature to be a gram negative bacteria and interacts better with the used positive charged toluidine blue compared to the gram positive *S. aureus*. These remarkable results confirm the potential of TOCNF as a scaffold for the development of new photoantimicrobial materials. Looking forward, the conjugation strategy developed in this work can be directly used to add an external photoantimicrobial coating layer to wood to prevent the proliferation of bacteria outdoors by sunlight irradiation.

3. Conclusion

Here, we demonstrated a successful development of an efficient light-mediated self-sterilizing cellulosic hybrid material. First the successful synthesis and characterization of two TOCNF samples doped with the photosensitizer TB was achieved, whereby TB was either covalently linked to the material (**1**) or physically adsorbed (**2**). The photophysical characterization of the materials reveals better oxygen accessibility to TB for the physically-adsorbed sample **2**, with the downside that TB may be washed out of the material when in contact with water. On the other hand, **1** shows much higher antibacterial activity than **2**, especially against *E. coli* under simulated solar irradiation, reducing its population by 4 $\log_{10}$ CFU mL^{-1} within 15 min of irradiation.

These results pave the way for the development of new single-use antibacterial surfaces. The covalent doping technology of nanocellulosic materials may be used to create antibacterial thin films on surfaces, which can trigger their activity under sunlight exposure.

Author statement

The manuscript "*Antimicrobial Efficacy of Solar Disinfection in Cellulose Fiber Supported Photoactive Materials*", submitted for publication in *Materials Today Communications*, has not been published, and it is not being considered for publication elsewhere than *Materials Today Communications*.

CRediT authorship contribution statement

Kostiainen Mauri A.: Conceptualization, Supervision, Validation, Writing – original draft, Writing – review & editing, Funding acquisition, Visualization. **Anaya-Plaza Eduardo:** Conceptualization, Funding acquisition, Supervision, Validation, Visualization, Writing – original draft, Writing – review & editing. **Fliri Lukas:** Methodology. **Nonell Santi:** Data curation, Formal analysis, Supervision, Validation, Writing – original draft, Writing – review & editing. **Bresolí-Obach Roger:** Data curation, Formal analysis, Investigation, Methodology, Supervision, Writing – original draft. **Solin Katariina:** Investigation, Methodology, Writing – original draft. **Jordà-Redondo Mireia:** Data curation, Investigation, Methodology, Writing – original draft. **Langerreiter Daniel:** Investigation, Methodology, Writing – original draft, Funding acquisition.

Declaration of Competing Interest

The authors declare that they have no known competing financial interests or personal relationships that could have appeared to influence the work reported in this paper.

Data availability

Data will be made available on request.

Acknowledgements

This work was a part of the Academy of Finland's Flagship Programme under Projects No. 318890 and 318891 (Competence Center for Materials Bioeconomy, FinnCERES), the Magnus Ehrnrooth foundation, the Academy of Finland (341057), and the Academy of Finland Centers of Excellence Program (2022– 2029) in Life-Inspired Hybrid Materials (LIBER). We acknowledge the provision of facilities and technical support by Aalto University Bioeconomy Facilities and OtaNano – Nanomicroscopy Center (Aalto-NMC).

This research was funded by the Spanish Agencia Estatal de Investigación and FEDER (grant number PID2020-115801RB-C22 and RYC2021-032773-I) and AGAUR (2020BP00066). S.N. thanks the Departament de Recerca i Universitats de la Generalitat de Catalunya for the support given to our research group (2021 SGR 01023) and the ICREA—Catalan Institution for Research and Advanced Studies for grant No. Ac2232308.

Experimental

The preparation and synthesis of the TOCNF, **1** and **2**, the purification of those materials, the quantum yield, the PDI assay with its additional graphs are included in the Supporting Information.

Appendix A. Supporting information

Supplementary data associated with this article can be found in the online version at doi:10.1016/j.mtcomm.2023.107858.

References

[1] J.C.O. Sardi, L. Scorzoni, T. Bernardi, A.M. Fusco-Almeida, M.J.S. Mendes Giannini, Candida species: current epidemiology, pathogenicity, biofilm formation, natural antifungal products and new therapeutic options, J. Med. Microbiol. 62 (2013) 10–24, https://doi.org/10.1099/jmm.0.045054-0.

[2] M. Wainwright, T. Maisch, S. Nonell, K. Plaetzer, A. Almeida, G.P. Tegos, M. R. Hamblin, Photoantimicrobials—are we afraid of the light, Lancet Infect. Dis. 17 (2017) e49–e55, https://doi.org/10.1016/S1473-3099(16)30268-7.

[3] M.R. Hamblin, Antimicrobial photodynamic inactivation: a bright new technique to kill resistant microbes, Curr. Opin. Microbiol. 33 (2016) 67–73, https://doi.org/10.1016/j.mib.2016.06.008.

[4] T.G. St. Denis, T. Dai, L. Izikson, C. Astrakas, R.R. Anderson, M.R. Hamblin, G. P. Tegos, All you need is light, Virulence 2 (2011) 509–520, https://doi.org/10.4161/viru.2.6.17889.

[5] E. Alves, M.A. Faustino, M.G. Neves, A. Cunha, J. Tome, A. Almeida, An insight on bacterial cellular targets of photodynamic inactivation, Future Med. Chem. 6 (2014) 141–164, https://doi.org/10.4155/fmc.13.211.

[6] R. Yin, T. Agrawal, U. Khan, G.K. Gupta, V. Rai, Y. Huang, M.R. Hamblin, Antimicrobial photodynamic inactivation in nanomedicine: small light strides against bad bugs, Nanomedicine 10 (2015) 2379–2404, https://doi.org/10.2217/nnm.15.67.

[7] N. Kashef, Y.Y. Huang, M.R. Hamblin, Advances in antimicrobial photodynamic inactivation at the nanoscale, Nanophotonics 6 (2017) 853–879, https://doi.org/10.1515/nanoph-2016-0189.

[8] M. Q. Mesquita, C. J. Dias, M.P.M.S. Neves, A. Almeida, M. F. Faustino, Revisiting current photoactive materials for antimicrobial photodynamic therapy, Molecules 23 (2018) 2424, https://doi.org/10.3390/molecules23102424.

[9] F. Vatansever, W.C.M.A. de Melo, P. Avci, D. Vecchio, M. Sadasivam, A. Gupta, R. Chandran, M. Karimi, N.A. Parizotto, R. Yin, G.P. Tegos, M.R. Hamblin, Antimicrobial strategies centered around reactive oxygen species – bactericidal antibiotics, photodynamic therapy, and beyond, FEMS Microbiol. Rev. 37 (2013) 955–989, https://doi.org/10.1111/1574-6976.12026.

[10] W.C. de Melo, P. Avci, M.N. de Oliveira, A. Gupta, D. Vecchio, M. Sadasivam, R. Chandran, Y.-Y. Huang, R. Yin, L.R. Perussi, G.P. Tegos, J.R. Perussi, T. Dai, M. R. Hamblin, Photodynamic inactivation of biofilm: taking a lightly colored approach to stubborn infection, Expert Rev. Anti Infect. Ther. 11 (2013) 669–693, https://doi.org/10.1586/14787210.2013.811861.
[11] O. Planas, E. Boix-Garriga, B. Rodríguez-Amigo, J. Torra, R. Bresolí-Obach, C. Flors, C. Viappiani, M. Agut, R. Ruiz-González, S. Nonell, Chapter 9. Newest approaches to singlet oxygen photosensitisation in biological media, in: Photochemistry, 2014: pp. 233–278. https://doi.org/10.1039/9781782624547–00233.
[12] G. Sridharan, A. Shankar, Toluidine blue: a review of its chemistry and clinical utility, J. Oral. Maxillofac. Pathol. 16 (2012) 251, https://doi.org/10.4103/0973-029X.99081.
[13] M. Bellinger, S. Sidhu, C. Rasmussen, Staining maize epidermal leaf peels with toluidine blue O, Bio-Protoc. 9 (2019) 1–11, https://doi.org/10.21769/BioProtoc.3214.
[14] L. Zhang, M. Williams, C.F. Poh, D. Laronde, J.B. Epstein, S. Durham, H. Nakamura, K. Berean, A. Hovan, N.D. Le, G. Hislop, R. Priddy, J. Hay, W.L. Lam, M.P. Rosin, Toluidine blue staining identifies high-risk primary oral premalignant lesions with poor outcome, Cancer Res. 65 (2005) 8017–8021, https://doi.org/10.1158/0008-5472.CAN-04-3153.
[15] N. Kashef, G. Ravaei Sharif Abadi, G.E. Djavid, Phototoxicity of phenothiazinium dyes against methicillin-resistant Staphylococcus aureus and multi-drug resistant Escherichia coli, Photo Photodyn. Ther. 9 (2012) 11–15, https://doi.org/10.1016/j.pdpdt.2011.11.004.
[16] N. Kashef, G. Ravaei Sharif Abadi, G.E. Djavid, Photodynamic inactivation of primary human fibroblasts by methylene blue and toluidine blue O, Photo Photodyn. Ther. 9 (2012) 355–358, https://doi.org/10.1016/j.pdpdt.2012.05.001.
[17] C.-P. Chen, C.-M. Hsieh, T. Tsai, J.-C. Yang, C.-T. Chen, Optimization and evaluation of a chitosan/hydroxypropyl methylcellulose hydrogel containing toluidine blue O for antimicrobial photodynamic inactivation, Int. J. Mol. Sci. 16 (2015) 20859–20872, https://doi.org/10.3390/ijms160920859.
[18] N. Kömerik, H. Nakanishi, A.J. MacRobert, B. Henderson, P. Speight, M. Wilson, In vivo killing of porphyromonas gingivalis by toluidine blue-mediated photosensitization in an animal model, Antimicrob. Agents Chemother. 47 (2003) 932–940, https://doi.org/10.1128/AAC.47.3.932-940.2003.
[19] X. Ragàs, T. Dai, G.P. Tegos, M. Agut, S. Nonell, M.R. Hamblin, Photodynamic inactivation of Acinetobacter baumannii using phenothiazinium dyes: in vitro and in vivo studies, Lasers Surg. Med. 42 (2010) 384–390, https://doi.org/10.1002/lsm.20922.
[20] Y. Habibi, H. Chanzy, M.R. Vignon, TEMPO-mediated surface oxidation of cellulose whiskers, Cellulose 13 (2006) 679–687, https://doi.org/10.1007/s10570-006-9075-y.
[21] Z. Tang, W. Li, X. Lin, H. Xiao, Q. Miao, L. Huang, L. Chen, H. Wu, TEMPO-oxidized cellulose with high degree of oxidation, Polymers 9 (2017) 421, https://doi.org/10.3390/polym9090421.
[22] T. Saito, Y. Nishiyama, J.-L. Putaux, M. Vignon, A. Isogai, Homogeneous suspensions of individualized microfibrils from TEMPO-catalyzed oxidation of native cellulose, Biomacromolecules 7 (2006) 1687–1691, https://doi.org/10.1021/bm060154s.
[23] E. Kontturi, P. Laaksonen, M.B. Linder, Nonappa, A.H. Gröschel, O.J. Rojas, O. Ikkala, Advanced materials through assembly of nanocelluloses, Adv. Mater. 30 (2018), 1703779, https://doi.org/10.1002/adma.201703779.
[24] T. Abitbol, A. Rivkin, Y. Cao, Y. Nevo, E. Abraham, T. Ben-Shalom, S. Lapidot, O. Shoseyov, Nanocellulose, a tiny fiber with huge applications, Curr. Opin. Biotechnol. 39 (2016) 76–88, https://doi.org/10.1016/j.copbio.2016.01.002.
[25] A. Kamdem Tamo, I. Doench, A. Morales Helguera, D. Hoenders, A. Walther, A. O. Madrazo, Biodegradation of crystalline cellulose nanofibers by means of enzyme immobilized-alginate beads and microparticles, Polymers 12 (2020) 1522, https://doi.org/10.3390/polym12071522.
[26] E. Kontturi, S. Spirk, Ultrathin films of cellulose: a materials perspective, Front. Chem. 7 (2019) 1–18, https://doi.org/10.3389/fchem.2019.00488.
[27] B.D. Mattos, B.L. Tardy, L.G. Greca, T. Kämäräinen, W. Xiang, O. Cusola, W.L. E. Magalhães, O.J. Rojas, Nanofibrillar networks enable universal assembly of superstructured particle constructs, Sci. Adv. 6 (2020) 1–11, https://doi.org/10.1126/sciadv.aaz7328.
[28] K. Oksman, Y. Aitomäki, A.P. Mathew, G. Siqueira, Q. Zhou, S. Butylina, S. Tanpichai, X. Zhou, S. Hooshmand, Review of the recent developments in cellulose nanocomposite processing, Compos. Part A Appl. Sci. Manuf. 83 (2016) 2–18, https://doi.org/10.1016/j.compositesa.2015.10.041.
[29] K. Yao, Q. Meng, V. Bulone, Q. Zhou, Flexible and responsive chiral nematic cellulose nanocrystal/poly(ethylene glycol) composite films with uniform and tunable structural color, Adv. Mater. 29 (2017), 1701323, https://doi.org/10.1002/adma.201701323.
[30] N. Lavoine, L. Bergström, Nanocellulose-based foams and aerogels: processing, properties, and applications, J. Mater. Chem. A. 5 (2017) 16105–16117, https://doi.org/10.1039/C7TA02807E.
[31] C. Aulin, E. Johansson, L. Wågberg, T. Lindström, Self-organized films from cellulose I nanofibrils using the layer-by-layer technique, Biomacromolecules 11 (2010) 872–882, https://doi.org/10.1021/bm100075e.
[32] E.D. Cranston, D.G. Gray, Morphological and optical characterization of polyelectrolyte multilayers incorporating nanocrystalline cellulose, Biomacromolecules 7 (2006) 2522–2530, https://doi.org/10.1021/bm0602886.
[33] R. Koppolu, J. Lahti, T. Abitbol, A. Swerin, J. Kuusipalo, M. Toivakka, Continuous processing of nanocellulose and polylactic acid into multilayer barrier coatings, ACS Appl. Mater. Interfaces 11 (2019) 11920–11927, https://doi.org/10.1021/acsami.9b00922.
[34] P. Chauhan, N. Yan, Novel bodipy—cellulose nanohybrids for the production of singlet oxygen, RSC Adv. 6 (2016) 32070–32073, https://doi.org/10.1039/C6RA04275A.
[35] M. Krouit, R. Granet, P. Branland, B. Verneuil, P. Krausz, New photoantimicrobial films composed of porphyrinated lipophilic cellulose esters, Bioorg. Med. Chem. 16 (2006) 1651–1655, https://doi.org/10.1016/j.bmcl.2005.12.008.
[36] E. Feese, H. Sadeghifar, H.S. Gracz, D.S. Argyropoulos, R.A. Ghiladi, Photobactericidal porphyrin-cellulose nanocrystals: synthesis, characterization, and antimicrobial properties, Biomacromolecules 12 (2011) 3528–3539, https://doi.org/10.1021/bm200718s.
[37] H. Hettegger, M. Gorfer, S. Sortino, A. Fraix, D. Bandian, C. Rohrer, W. Harreither, A. Potthast, T. Rosenau, Synthesis, characterization and photo-bactericidal activity of silanized xanthene-modified bacterial cellulose membranes, Cellulose 22 (2015) 3291–3304, https://doi.org/10.1007/s10570-015-0715-y.
[38] C. Ringot, V. Sol, M. Barrière, N. Saad, P. Bressollier, R. Granet, P. Couleaud, C. Frochot, P. Krausz, Triazinyl porphyrin-based photoactive cotton fabrics: preparation, characterization, and antibacterial activity, Biomacromolecules 12 (2011) 1716–1723, https://doi.org/10.1021/bm200082d.
[39] J.-P. Mbakidi, K. Herke, S. Alvès, V. Chaleix, R. Granet, P. Krausz, S. Leroy-Lhez, T.-S. Ouk, V. Sol, Synthesis and photobiocidal properties of cationic porphyrin-grafted paper, Carbohydr. Polym. 91 (2013) 333–338, https://doi.org/10.1016/j.carbpol.2012.08.013.
[40] T. Wang, L. Xu, H. Shen, X. Cao, Q. Wei, R.A. Ghiladi, Q. Wang, Photoinactivation of bacteria by hypocrellin-grafted bacterial cellulose, Cellulose 27 (2020) 991–1007, https://doi.org/10.1007/s10570-019-02852-9.
[41] X. Liu, M. Wu, M. Wang, Q. Hu, J. Liu, Y. Duan, B. Liu, Direct synthesis of photosensitizable bacterial cellulose as engineered living material for skin wound repair, Adv. Mater. 34 (2022), 2109010, https://doi.org/10.1002/adma.202109010.
[42] R. Koshani, J. Zhang, T.G.M. van de Ven, X. Lu, Y. Wang, Modified hairy nanocrystalline cellulose as photobactericidal nanofillers for food packaging application, ACS Sustain. Chem. Eng. 9 (2021) 10513–10523, https://doi.org/10.1021/acssuschemeng.1c02289.
[43] T. Czapka, A. Winkler, I. Maliszewska, R. Kacprzyk, Fabrication of photoactive electrospun cellulose acetate nanofibers for antibacterial applications, Energies 14 (2021) 2598, https://doi.org/10.3390/en14092598.
[44] L. George, A. Hiltunen, V. Santala, A. Efimov, Photo-antimicrobial efficacy of zinc complexes of porphyrin and phthalocyanine activated by inexpensive consumer LED lamp, J. Inorg. Biochem. 183 (2018) 94–100, https://doi.org/10.1016/j.jinorgbio.2018.03.015.
[45] E. Anaya-Plaza, E. van de Winckel, J. Mikkilä, J.-M. Malho, O. Ikkala, O. Gulías, R. Bresolí-Obach, M. Agut, S. Nonell, T. Torres, M.A. Kostiainen, A. de la Escosura, Photoantimicrobial biohybrids by supramolecular immobilization of cationic phthalocyanines onto cellulose nanocrystals, Chem. A Eur. J. 23 (2017) 4320–4326, https://doi.org/10.1002/chem.201605285.
[46] V. Decraene, J. Pratten, M. Wilson, Cellulose acetate containing toluidine blue and rose bengal is an effective antimicrobial coating when exposed to white light, Appl. Environ. Microbiol. 72 (2006) 4436–4439, https://doi.org/10.1128/AEM.02945-05.
[47] M. Vuoriluoto, H. Orelma, M. Lundahl, M. Borghei, O.J. Rojas, Filaments with affinity binding and wet strength can be achieved by spinning bifunctional cellulose nanofibrils, Biomacromolecules 18 (2017) 1803–1813, https://doi.org/10.1021/acs.biomac.7b00256.
[48] K. Solin, M. Vuoriluoto, A. Khakalo, T. Tammelin, Cannabis detection with solid sensors and paper-based immunoassays by conjugating antibodies to nanocellulose, Carbohydr. Polym. 304 (2023), 120517, https://doi.org/10.1016/j.carbpol.2022.120517.
[49] X.-Q. Wang, Q. Lei, J.-Y. Zhu, W.-J. Wang, Q. Cheng, F. Gao, Y.-X. Sun, X.-Z. Zhang, Cucurbit[8]uril regulated activatable supramolecular photosensitizer for targeted cancer imaging and photodynamic therapy, ACS Appl. Mater. Interfaces 8 (2016) 22892–22899, https://doi.org/10.1021/acsami.6b07507.
[50] J. Chen, T.C. Cesario, P.M. Rentzepis, Time resolved spectroscopic studies of methylene blue and phenothiazine derivatives used for bacteria inactivation, Chem. Phys. Lett. 498 (2010) 81–85, https://doi.org/10.1016/j.cplett.2010.08.042.
[51] S. Nonell, S.E. Braslavsky, [4] Time-resolved singlet oxygen detection. Methods in Enzymology, Academic Press, 2000, pp. 37–49, https://doi.org/10.1016/S0076-6879(00)19006-8.
[52] A. Jiménez-Banzo, X. Ragàs, P. Kapusta, S. Nonell, Time-resolved methods in biophysics. 7. Photon counting vs. analog time-resolved singlet oxygen phosphorescence detection, Photochem. Photobiol. Sci. 7 (2008) 1003–1010, https://doi.org/10.1039/b804333g.
[53] J.R. Harbour, S.L. Issler, Involvement of the azide radical in the quenching of singlet oxygen by azide anion in water, J. Am. Chem. Soc. 104 (1982) 903–905, https://doi.org/10.1021/ja00367a066.
[54] F. Wilkinson, J.G. Brummer, Rate constants for the decay and reactions of the lowest electronically excited singlet state of molecular oxygen in solution, J. Phys. Chem. Ref. Data. 10 (1981) 809–999, https://doi.org/10.1063/1.555655.
[55] N.S. Soukos, M. Wilson, T. Burns, P.M. Speight, Photodynamic effects of toluidine blue on human oral keratinocytes and fibroblasts andStreptococcus sanguis evaluated in vitro, Lasers Surg. Med. 18 (1996) 253–259, https://doi.org/10.1002/(SICI)1096-9101(1996)18:3<253::AID-LSM6>3.0.CO;2-R.
[56] R.F. Donnelly, P.A. McCarron, M.M. Tunney, A. David Woolfson, Potential of photodynamic therapy in treatment of fungal infections of the mouth. Design and

characterisation of a mucoadhesive patch containing toluidine blue O, J. Photochem. Photobiol. B Biol. 86 (2007) 59–69, https://doi.org/10.1016/j.jphotobiol.2006.07.011.

[57] G.G. Carvalho, M.P. Felipe, M.S. Costa, The photodynamic effect of methylene blue and toluidine blue on Candida albicans is dependent on medium conditions, J. Microbiol 47 (2009) 619–623, https://doi.org/10.1007/s12275-009-0059-0.

[58] R.C. Souza, J.C. Junqueira, R.D. Rossoni, C.A. Pereira, E. Munin, A.O.C. Jorge, Comparison of the photodynamic fungicidal efficacy of methylene blue, toluidine blue, malachite green and low-power laser irradiation alone against Candida albicans, Lasers Med Sci. 25 (2010) 385–389, https://doi.org/10.1007/s10103-009-0706-z.

[59] H.-F. Chien, C.-P. Chen, Y.-C. Chen, P.-H. Chang, T. Tsai, C.-T. Chen, The use of chitosan to enhance photodynamic inactivation against Candida albicans and its drug-resistant clinical isolates, Int. J. Mol. Sci. 14 (2013) 7445–7456, https://doi.org/10.3390/ijms14047445.

[60] R. Wiench, J. Nowicka, M. Pajączkowska, P. Kuropka, D. Skaba, A. Kruczek-Kazibudzka, A. Kuśka-Kiełbratowska, K. Grzech-Leśniak, Influence of incubation time on ortho-toluidine blue mediated antimicrobial photodynamic therapy directed against selected Candida strains—an in vitro study, Int. J. Mol. Sci. 22 (2021) 10971, https://doi.org/10.3390/ijms222010971.

[61] C.A. Gueymard, D. Myers, K. Emery, Proposed reference irradiance spectra for solar energy systems testing, Sol. Energy 73 (2002) 443–467, https://doi.org/10.1016/S0038-092X(03)00005-7.